

Mixed action with Borici-Creutz fermions on staggered sea

S. Basak¹, D. Chakrabarti², J. Goswami²

¹*School of Physical Sciences, NISER Bhubaneswar, Khurda-752050, India.*

²*Department of Physics, Indian Institute of Technology Kanpur, Kanpur-208016, India*

(Dated: April 7, 2021)

Abstract

Mixed action lattice QCD with Borici-Creutz valence quarks on staggered sea is investigated. The counter terms in Borici-Creutz action are fixed nonperturbatively to restore the broken parity and time symmetries. When symmetries are restored, the usual signatures of partial quenching are recovered. We find the scalar correlators to be negative for lower valence quark masses but the errorbars are rather large when their mean values are negative at earlier time slices. The size of unitarity violation due to different discretization of valence and sea quark is determined by measuring Δ_{mix} and is found to be comparable with other mixed action studies.

PACS numbers: 11.15.Ha, 11.30.Rd

I. INTRODUCTION

Minimally doubled fermions are promising techniques to study light quarks on lattice. They are known to preserve chiral symmetry for a degenerate quark doublet and are local. This can be helpful for $N_f = 2$ lattice simulations, and is relatively simpler and possibly faster than Ginsparg-Wilson fermions. There are two main realizations of the minimally doubled fermions – Karsten-Wilczek [1, 2] and Borici-Creutz [3, 4]. In this paper, we study mixed action lattice QCD with Borici-Creutz valence quarks in Asqtad improved staggered sea, restricting to light quarks only.

Motivated by the fact that electrons on a graphene lattice are described by a massless Dirac-like equation (quasi-relativistic Dirac equation), Creutz proposed a four dimensional Euclidean lattice action describing two flavors of fermion, centered at $\pm p_\mu$ in the momentum space [3]. The action was defined on a honeycomb or graphene lattice with tunable parameters to control the magnitude of p_μ . Borici found a solution for the parameters such that the two flavors are located at $p = (0, 0, 0, 0)$ and $(\pi/2, \pi/2, \pi/2, \pi/2)$. The chirally invariant Borici-Creutz action breaks hypercubic symmetry leading to the breaking of discrete symmetries like parity and time-reversal [5, 6]. This introduces non-covariant counterterms through quantum corrections. The renormalization properties of the BC fermion at one loop in perturbation theory have been investigated in [7, 8]. It was shown that in presence of gauge background with integer-valued topological charge, BC action satisfies the Atiyah-Singer index theorem [9]. The cut-off effects on BC fermions at the tree-level of perturbation theory has been studied by K. Cichy et. al.[10].

However, there is a dearth of numerical studies with Borici-Creutz fermions and very few literatures which would suggest its usefulness and performance in lattice QCD simulations. In recent times, we have initiated a series of detailed numerical studies to ascertain its viability in lattice simulations. Using Borici-Creutz fermions we have studied discrete chiral symmetry breaking in a two dimensional Gross-Neveu model [11] and the mass spectroscopy in 2-dimensional field theories [12] in lattice. In this work, we extend our investigations to 4-dimensional lattice and attempt to simulate QCD with Borici-Creutz action. Here, we consider a mixed action approach with Borici-Creutz valence quarks on an Asqtad improved staggered sea. The coefficients of the counterterms of the renormalized action are fixed non-perturbatively to restore the broken hypercubic symmetry of the Borici-Creutz action.

At finite lattice spacing, mixed action QCD violates unitarity but it is believed to have the correct continuum limit. In mixed action, proper matching of the sea and valence actions is important. One can tune the valence quark masses to have the desired meson masses in the mixed action to agree with QCD with unitarity. Since the valence and sea quarks have different discretization effects, it is not, however, possible to tune the mesons made up of purely valence and sea quarks to restore unitarity at finite lattice spacing. Alternatively, one can correct the mismatch in the bare parameters using partially quenched mixed action approach in which the actions are not matched but the parameters are tuned to reproduce the physical observables[23].

The scalar correlator is known to be sensitive to the unitarity violation, due to different discretization of valence and sea quarks, because of two mesons intermediate states in the hair-pin diagram. After the counterterms are tuned and the breaking of the hypercubic symmetry minimized, the scalar correlator shows the effect of partially quenched QCD and becomes negative for valence quark mass smaller than sea quark mass ($m_{\text{val}} < m_{\text{sea}}$). The quark mass dependence of pion mass squared is found to be linear for heavier quarks but logarithmic corrections as predicted by one loop chiral perturbation theory become prominent for lighter quarks. The lattice result for the pion mass agrees well with the one loop partially quenched chiral perturbation prediction. There are several studies of mixed action lattice QCD with different combinations of sea and valence quarks [13–23]. Many of these studies use Asqtad staggered sea quarks.

In the leading order mixed action chiral perturbation theory, a lattice spacing dependent low energy constant Δ_{mix} appears as a free parameter in the mass formula for meson made up of one valence and one sea quark. The Δ_{mix} gives a measure of the unitarity violation. (In this paper we actually calculate $\tilde{\Delta}_{\text{mix}}$ which is different from Δ_{mix} by an additional term as will be explained later in the text in Sec.VI.) The Δ_{mix} obtained in this work is found to be comparable to the mixed action with domain wall fermions on staggered sea [13, 14]. Fermions based on the solutions of Ginsparg-Wilson relation, such as Domain-wall or Overlap fermions, are in general computationally very demanding but Borici-Creutz fermions being ultra local is expected to be computationally cheaper. So, it raises the hope that Borici-Creutz fermion might be a good alternative for QCD simulations with dynamical fermions.

II. BORICI-CREUTZ ACTION AND POINT SPLIT METHOD

The free Borici-Creutz action in discretized 4 dimensional space-time lattice is written as,

$$S_{BC} = \sum_x \left[\frac{1}{2} \sum_{\mu} \bar{\psi}(x) \gamma_{\mu} (\psi(x + \hat{\mu}) - \psi(x - \hat{\mu})) - \frac{i}{2} \sum_{\mu} \bar{\psi}(x) (\Gamma - \gamma_{\mu}) (2\psi(x) - \psi(x + \hat{\mu}) - \psi(x - \hat{\mu})) + m \bar{\psi}(x) \psi(x) \right] \quad (1)$$

where, $\Gamma = \frac{1}{2}(\gamma_1 + \gamma_2 + \gamma_3 + \gamma_4)$, $\{\Gamma, \gamma_{\mu}\} = 1$ and we have taken lattice spacing $a = 1$. In the momentum space, the action turns out to be diagonal and is,

$$S_{BC} = \int \frac{d^4 p}{(2\pi)^4} \bar{\psi}(p) \left[\sum_{\mu} (\gamma_{\mu} \sin(p_{\mu}) + i(\Gamma - \gamma^{\mu}) \cos(p_{\mu})) - 2i\Gamma + m \right] \psi(p). \quad (2)$$

The zeroes of the free massless Dirac operator are at $(0, 0, 0, 0)$ and $(\pi/2, \pi/2, \pi/2, \pi/2)$. The spinor $\psi(p)$ contains two degenerate flavors. We can construct the fields for these two flavors at two different poles by the method of point splitting [24–26]. We define

$$d(p) \equiv \frac{1}{4} \Gamma \sum_{\mu} (1 - \sin p_{\mu}) \psi(p)$$

$$u(p) \equiv \frac{1}{4} \sum_{\mu} (1 - \cos(p_{\mu} + \pi/2)) \psi(p + \pi/2) \quad (3)$$

$$\Rightarrow u(p - \pi/2) = \frac{1}{4} \sum_{\mu} (1 - \cos p_{\mu}) \psi(p), \quad (4)$$

such that $d(0) = \Gamma \psi(0)$ and $d(\pi/2) = 0$ implying d is defined as an excitation around the pole at $(0, 0, 0, 0)$. Similarly, $u(0) = \psi(\pi/2)$ is defined around the pole at $(\pi/2, \pi/2, \pi/2, \pi/2)$. The flavors are defined within an energy region, for d quark we define a region in the momentum space such that the energy $E < \pi/4$ and for the u quark $E > \pi/4$, so that there is no overlap between these two fields. The definition of these fields are, however, not unique. One can also choose a different prescription,

$$d(p) \equiv \Gamma \prod_{\mu} (1 - \sin p_{\mu}) \psi(p)$$

$$u(p - \pi/2) \equiv \prod_{\mu} (1 - \cos p_{\mu}) \psi(p). \quad (5)$$

These two set of definitions of Eq. 3 and Eq. 5 are equivalent to each other, but we found that the spectrum obtained using the product form of fields in Eq. 5 to be noisier compared to those obtained from Eq. 3. Therefore, in our work we have implemented the point split

fields as defined in Eq. 3, where the summation over the Lorentz index μ is carried out. The Γ factor in d -field is inserted since the chiral symmetry is flavored *i.e.*, u and d have a relative minus sign under γ_5 transformation.

The Borici-Creutz action Eq. 1 has a special direction in Euclidean space which is the major hypercube diagonal (the line joining the two zeros) given by Γ . The action is symmetric under the cubic subgroup of the hypercubic group which preserves the special direction. This breaks the reflection symmetry of the hypercube leading to the breaking of parity and time symmetry[5]. Because of the broken hypercubic symmetry, the counterterms are necessary for a renormalized theory. The allowed counterterms for the Borici-Creutz action are dimension-4 counterterm $c_4(g_0) \bar{\psi} \Gamma \sum_{\mu} D_{\mu} \psi$ and dimension-3 counterterm $ic_3(g_0) \bar{\psi} \Gamma \psi$ (for a discussion of counterterms in the context of minimally doubled fermions see [8]). Then the complete renormalized action, with the gauge interaction turned on, reads

$$\begin{aligned}
S_{BC} = \sum_x \left[\frac{1}{2} \sum_{\mu} \left(\bar{\psi}(x) (\gamma_{\mu} + c_4(g_0) \Gamma + i\gamma'_{\mu}) U_{\mu}(x) \psi(x + \hat{\mu}) \right. \right. \\
\left. \left. - \bar{\psi}(x + \hat{\mu}) (\gamma_{\mu} - c_4(g_0) \Gamma - i\gamma'_{\mu}) U_{\mu}^{\dagger}(x) \psi(x) \right) \right. \\
\left. + \bar{\psi}(x) (m + i\tilde{c}_3(g_0) \Gamma) \psi(x) \right], \tag{6}
\end{aligned}$$

where, $\tilde{c}_3 = c_3 - 2$, $\gamma'_{\mu} = \Gamma - \gamma_{\mu} = \Gamma \gamma_{\mu} \Gamma$ and g_0 is the bare coupling parameter. The coefficients of the dimension-3 and 4 counterterms, c_3 and c_4 respectively, have been evaluated in 1-loop lattice perturbation theory [8] and are given by,

$$\begin{aligned}
c_3(g_0) &= 29.54170 \cdot \frac{g_0^2}{16\pi^2} C_F + \mathcal{O}(g_0^4), \\
c_4(g_0) &= 1.52766 \cdot \frac{g_0^2}{16\pi^2} C_F + \mathcal{O}(g_0^4). \tag{7}
\end{aligned}$$

The mixed action study has been carried out with the above renormalized Borici-Creutz action(Eq. 6) for the valence quarks.

A. Simulation details

The mixed action simulation is carried out with Borici-Creutz fermions on three ensembles of publicly available MILC lattices with 2+1 dynamical flavors of Asqtad improved staggered fermions [27], with a fixed ratio $am_l/am_s = 1/5$. The details of the MILC configurations used in this work are listed in Table I. We generated the staggered sea quark propagators

Lattice dim.	$\beta = 10/g_0^2$	am_l/am_s	a (fm)	volume (fm) ³	# configs
$16^3 \times 48$	6.572	0.0097 / 0.0484	≈ 0.15	$\sim (2.4 \text{ fm})^3$	40
$20^3 \times 64$	6.76	0.01 / 0.05	≈ 0.13	$\sim (2.6 \text{ fm})^3$	40
$28^3 \times 96$	7.09	0.0062 / 0.031	≈ 0.09	$\sim (2.5 \text{ fm})^3$	30

TABLE I: Details of MILC lattices [27] used in this work.

with sea quark mass m_l and m_s which are required for construction of the mixed valence-sea mesons. The number of configurations used are determined by the limitations of our computational resources and by the reasonable size of statistical errors of the meson masses. Since the measurement of $a^2 \Delta_{\text{mix}}$ is one of the important parts of this study, we prefer to use lattices of three different spacings in lieu of multiple am_l/am_s ratios (for a fixed lattice spacing) as it has been shown in multiple studies that Δ_{mix} does not depend significantly on the sea masses [17].

The Borici-Creutz valence quark propagators are constructed using a range of bare quark masses $[0.0075 - 0.5]$ which restricts the $m_\pi L$ around 4 and we think best suited to study the chiral logs and partial quenching. The strange mass is tuned by setting the fictitious $s\bar{s}$ pseudoscalar mass to 682 MeV [28]. Similar strange mass is also obtained by using $m_{\text{ps}}/m_{\text{vec}} = 0.673$ [27] for tuning. Random wall sources are used for the generation of all quark propagators. Both the APE and HYP smearing of the MILC lattices are tried but no significant advantages have been observed. The meson masses are extracted by fitting the meson propagators with double exponential ansatz. All the fits are uncorrelated and the errors are from Jack-knife analysis.

III. NON-PERTURBATIVE FIXING OF THE COUNTER TERMS

A. Parity condensate

The Borici-Creutz fermions exhibit parity-flavor breaking, which follows from absence of the hypercubic symmetry of the action in Eq. 1. As because the CPT is conserved, the T -symmetry is also broken. Consequently the counterterms are necessary for renormalized theory and those that are allowed by the remaining symmetry are added to the action. In the present case, as discussed before, two such counterterms of dimension-3 and 4 are introduced.

The coefficients of these operators, $\tilde{c}_3(g_0)$ and $c_4(g_0)$, can then be tuned to restore the desired symmetries. These coefficients depend on the gauge coupling, the expressions for which in 1-loop lattice perturbation theory are given in Eq. 7. This means these values will be different for different lattices. The perturbative values of the coefficients corresponding to the three lattices that we use in this work, are given in the Table II.

Lattice size	$16^3 \times 48$	$20^3 \times 64$	$28^3 \times 96$
\tilde{c}_3	-1.6211	-1.632	-1.649
c_4	0.0196	0.0189	0.0181

TABLE II: Perturbative values for \tilde{c}_3 and c_4

We expect the values of \tilde{c}_3 and c_4 , needed to restore the symmetries of the action, to be different on the lattices we use from the perturbative values. In this work, the tuning of these counterterm coefficients is achieved by minimizing the parity breaking and time asymmetry.

The quantity we measure to determine the size of parity breaking is the parity condensate $|\langle \bar{\psi} i \gamma_5 \tau_3 \psi \rangle|$, where τ_3 is the third generator of $SU(2)$. First we study the variation of the chiral condensate as we tune \tilde{c}_3 keeping c_4 fixed at its perturbative value for the lattice in use. The dependence of parity condensate on \tilde{c}_3 for various lattices is shown in Fig.1. The minimum of the condensate for all three ensembles appears around $\tilde{c}_3 = -0.5$. Besides, the actual values and the minimum of parity condensate appear to have very less dependence on the lattice spacing.

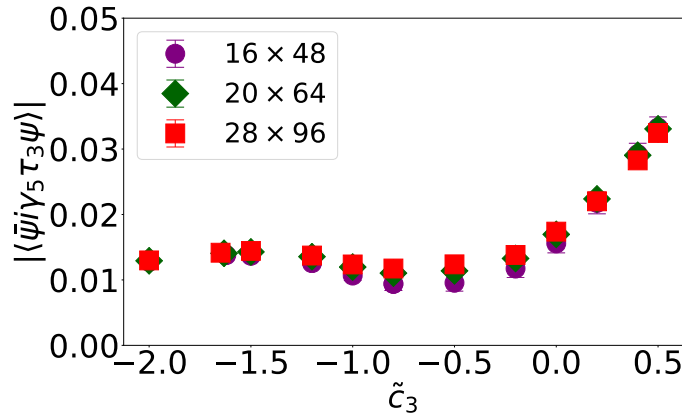


FIG. 1: Parity condensate versus \tilde{c}_3 for $c_4 = 0.0196, 0.0189$ and 0.0181 on $16^3 \times 48, 20^3 \times 64$ and $28^3 \times 96$ lattices respectively.

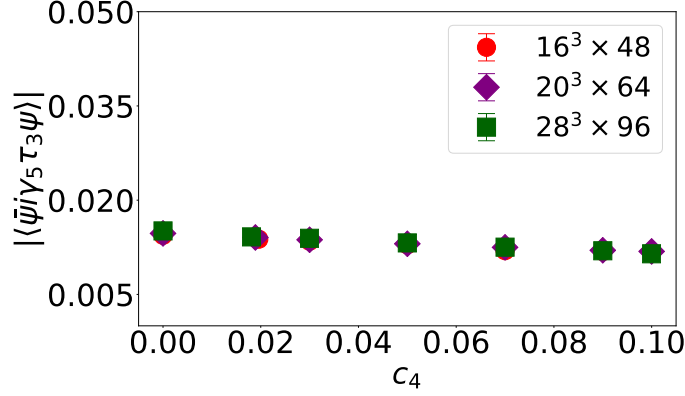


FIG. 2: Parity condensate versus c_4 for $\tilde{c}_3 = -0.5$ on $16^3 \times 48$, $20^3 \times 64$ and $28^3 \times 96$ lattices.

In the next step, we fix \tilde{c}_3 to this non-perturbative value and measure parity condensate for varying c_4 . This is plotted in Fig.2. We observe very little dependence of parity condensate on c_4 for all the three lattices. We have checked that this nature is also true for other values of \tilde{c}_3 . Here too we find that the parity condensate is almost independent of the lattice spacing. Therefore, tuning \tilde{c}_3 alone is sufficient for minimizing the breaking of parity.

B. Time asymmetry

The Borici-Creutz action has PT -symmetry and, because of breaking of parity, we expect to see sign of time asymmetry in the theory and lattice calculation. In lattice simulation, this time asymmetry can show up in the spectrum and manifests through non-degeneracy of forward and backward propagating meson states.

The pion propagators and the corresponding effective masses for different c_4 , while keeping \tilde{c}_3 fixed at -0.5 as obtained above, are shown in Fig.3. The pion operator is constructed from the d -quark field as defined in Eq. 3. The asymmetry in the forward and backward propagating parts and consequently difference in effective masses is rather evident. The asymmetry in pion propagators and the mass difference vanishes when c_4 is lowered to about 0.005. This behavior does not change with the changing values of \tilde{c}_3 implying that the size of time symmetry breaking is almost entirely driven by c_4 . Additionally, the value of c_4 at which the time symmetry is restored remain fairly constant for all the three lattices that we used. To ascertain that \tilde{c}_3 has practically no role in restoring time symmetry, we carried out the above experiment for various values of \tilde{c}_3 keeping $c_4 = 0.005$ fixed. The

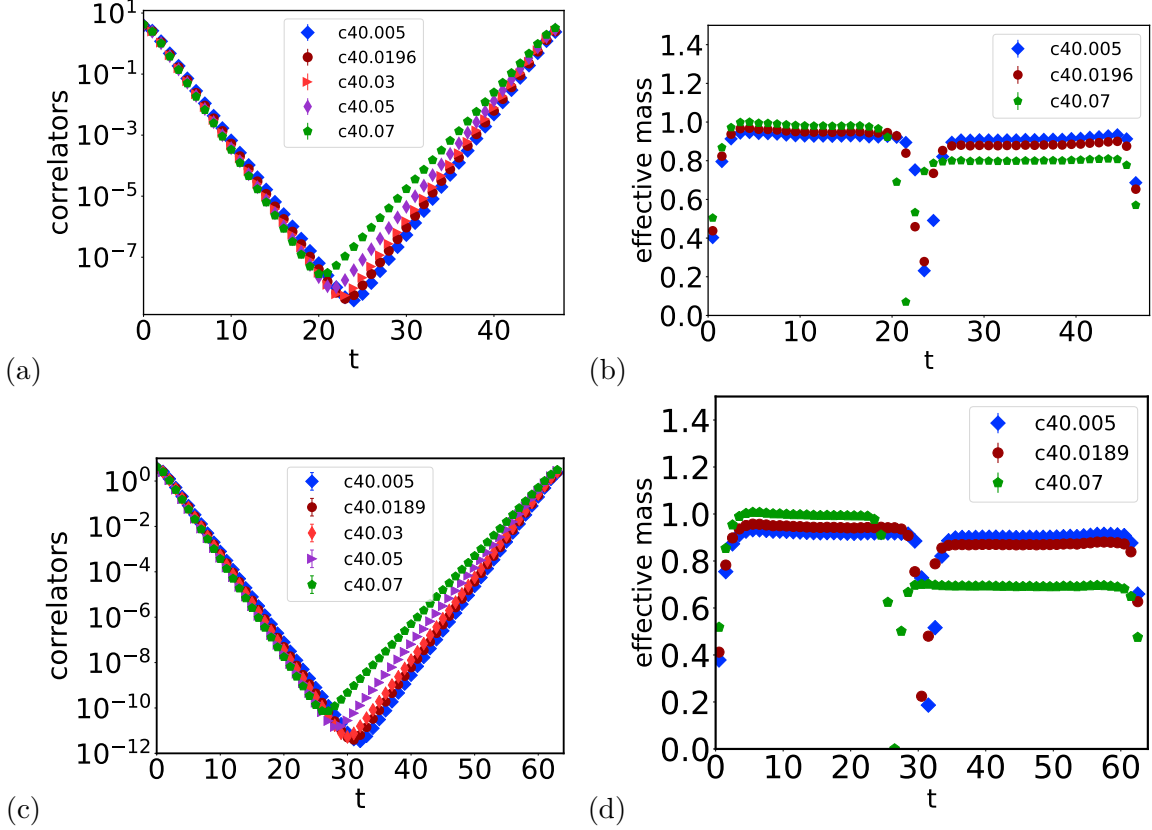


FIG. 3: Pion correlator and effective mass for different values of c_4 keeping $\tilde{c}_3 = -0.5$ fixed. Plots in upper panel (a) and (b) are for $16^3 \times 48$ lattices and lower panel (c) and (d) are for $20^3 \times 64$ lattices. Similar results for $28^3 \times 96$ lattices are not shown here.

plots in Fig. 4 show no asymmetry in pion correlators over the time slices neither any mass difference between forward and backward propagating pions.

In Fig.5, we plot the mass difference of the forward and backward propagating pion masses against the variation of c_4 while keeping $\tilde{c}_3 = -0.5$ in (a) while in (b) the variation against \tilde{c}_3 is shown keeping c_4 fixed at 0.005. Fig. 5(b) clearly indicates absence of any role of \tilde{c}_3 in restoring time symmetry. Also the plot shows, although the mass differences are different for different lattices in absence of time symmetry, the mass differences converge to zero at about $c_4 = 0.005$ upon restoration of symmetry. The smallness of c_4 suggests that T -symmetry is only weakly broken. Besides, the values of \tilde{c}_3 and c_4 thus tuned are significantly different from their 1-loop values as given in Table II. Henceforth, we have used $\tilde{c}_3 = -0.5$ and $c_4 = 0.005$ in all our subsequent simulations irrespective of lattice ensembles. The renormalization counter terms should not be observable dependent, once the counterterms are tuned nonpertubatively which in principle include all orders of perturbation theory to

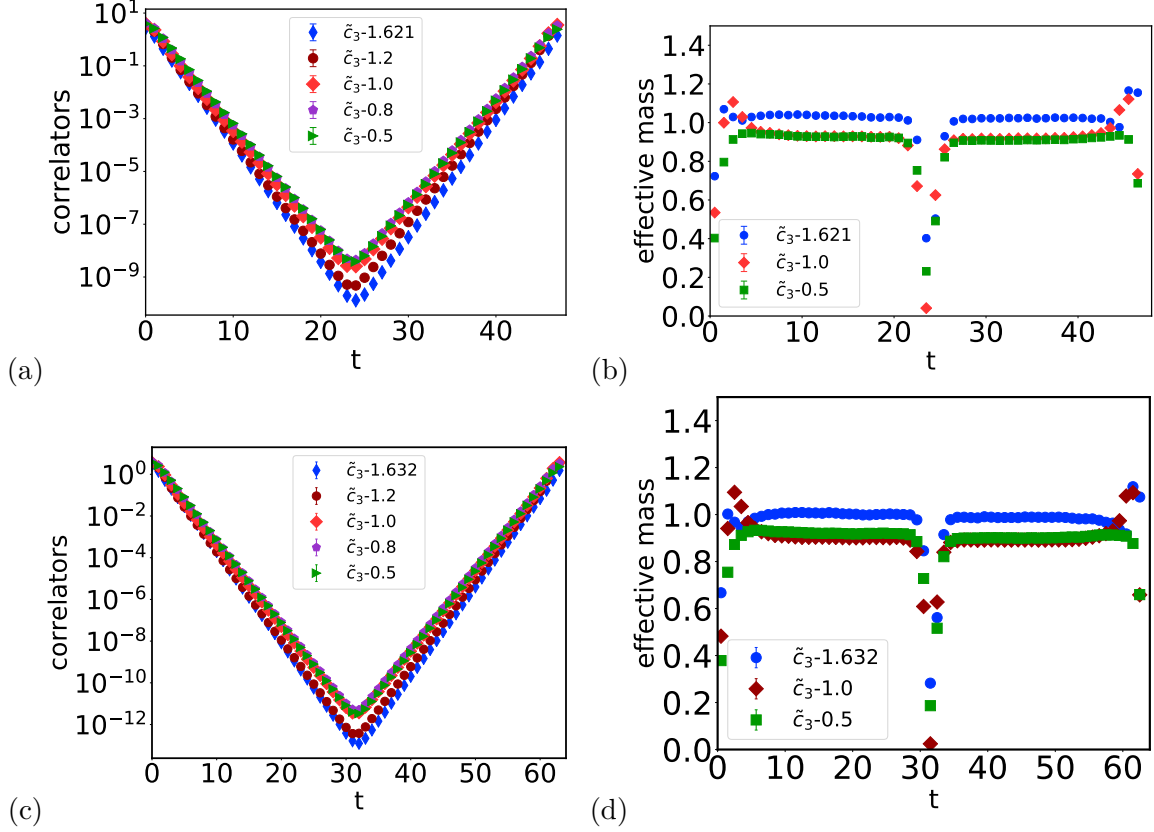


FIG. 4: Pion correlator and effective mass for different values of \tilde{c}_3 at fixed $c_4 = 0.005$. (a) and (b) for $16^3 \times 48$ lattice, (c) and (d) for $20^3 \times 64$ lattice.

restore the broken symmetries using certain observables, we expect that there will be no more symmetry breaking effects in other observables too. The pathologies of chiral perturbation theory with P , T symmetries e.g., chiral log in pion mass or negative scalar correlator due to partial quenching in mixed action etc are also observed with the renormalized BC action as expected. We have also measured various pseudoscalar and vector mesons for the GMOR and $SU(6)$ mass formula, which appear in the following section, and their behavior are consistent with other lattice fermions.

IV. MIXED ACTION PION MASS

Having tuned the counterterm coefficients, we next turn to the pion spectrum. Both the d and u quark fields, defined in Eq. 3, can be used to construct meson $q\bar{q}$ operators but they give identical results. Here we exclusively quote the results for $d\bar{d}$ mesons. The pion spectrum is obtained for valence quark mass in the range of $[0.0075 - 0.5]$. In Fig.6(a) and

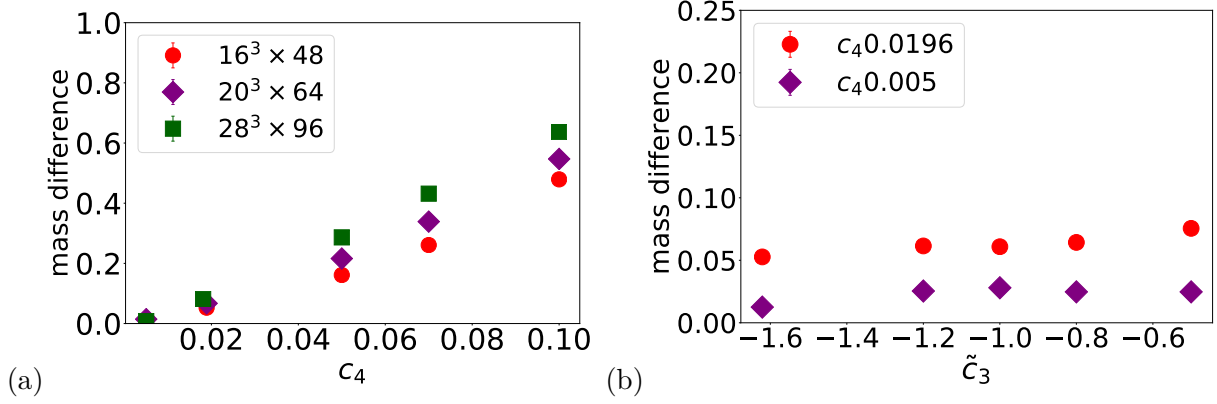


FIG. 5: Variations of forward-backward mass difference with the coefficients of the counter terms. (a) Variation with c_4 when $\tilde{c}_3 = -0.5$ for $16^3 \times 48$, $20^3 \times 64$, and $28^3 \times 96$ lattices. (b) Variation with \tilde{c}_3 for $c_4 = 0.0196$, 0.005 on $16^3 \times 48$ lattice.

(b), we plotted the pion mass m_π and pion mass squared m_π^2 respectively as function of bare valence quark mass m . At small quark masses, the plot deviates from straight line due to the logarithmic correction coming from one loop chiral perturbation theory,

$$m_\pi^2 = 2Bm + (2B)^2 \frac{m^2}{(32\pi^2 f^2)} \log(m) \quad , \quad (8)$$

where B is the LEC and f is the pion decay constant. The chiral log has been studied previously for different lattice fermions in the context of mixed action in [29–31]. A more complete mass formula in one loop partially quenched chiral perturbation theory is given by [30, 32],

$$m_\pi^2 = C_1 m + C_{1L} m \log(m) + C_2 m^2 + C_{2L} m^2 \log(m), \quad (9)$$

where C_1 , C_{1L} , C_2 , C_{2L} are independent low energy constants. The existence of chiral log in our mixed action simulation is more prominently visible when the ratio of m_π^2/m is plotted against m . Here we chose to show the results from only $20^3 \times 64$ lattice to avoid repetitions.

We plot in Fig.6(b) the results for m_π^2/m versus m for the same range of quark mass to highlight the evidence of the partially quenched chiral logarithm due to mismatch of valence and sea quark masses. In the same plot we show the fitting of our results with the PQ χ PT formula of Eq. 9. Here, however, away from the smaller quark mass the m_π^2/m attains some sort of plateau and is expected to rise at still higher masses.

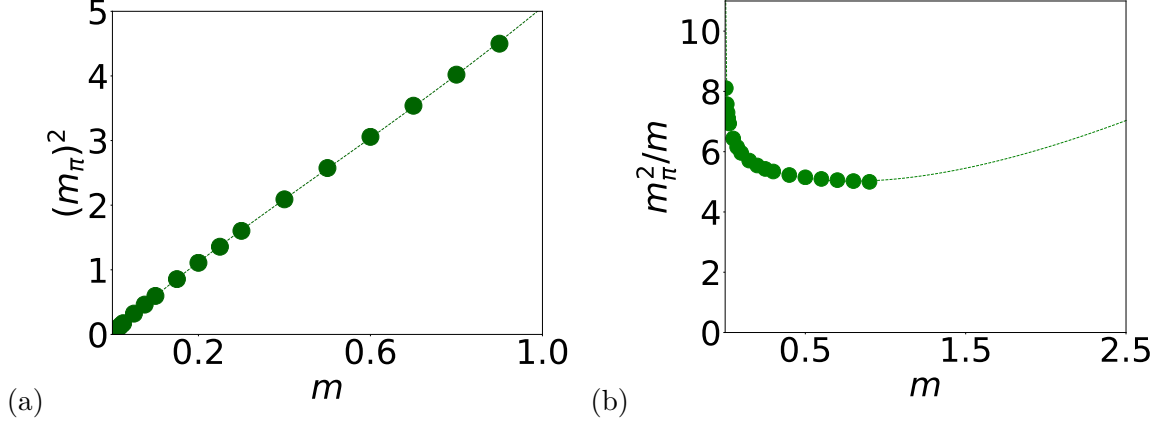


FIG. 6: Pion mass-squared as a function of valence quark mass m on $20^3 \times 64$ lattice. Error bars are smaller than the symbol size. In (b), the dotted curve is a fit to the mass formula in Eq. 9.

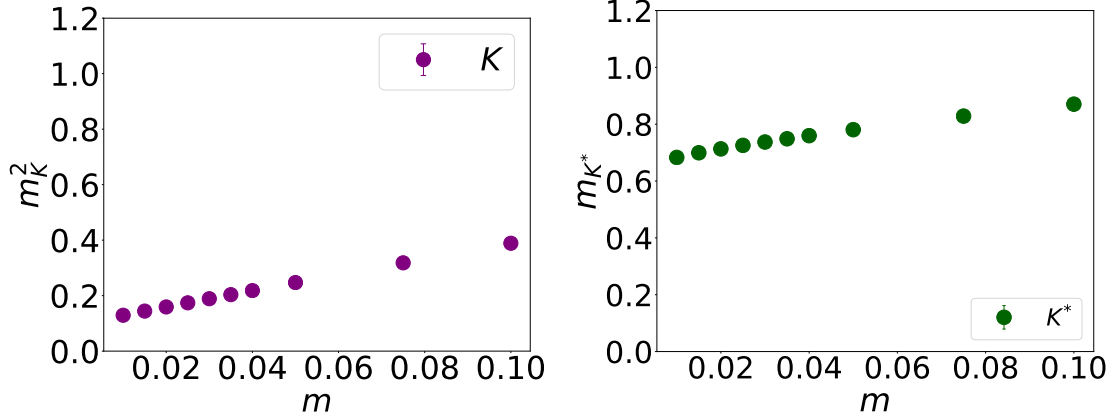


FIG. 7: m_K^2 and m_{K^*} versus light quark mass on $20^3 \times 64$ lattice.

Generally, the strange quark mass is determined by tuning the unphysical pseudoscalar $s\bar{s}$ meson mass to 687 MeV. Having the same quantum number, $s\bar{s}$ mixes with $u\bar{u}$ and $d\bar{d}$ to produce η and η' mesons. But purely $s\bar{s}$ meson is obtained by omitting the quark-antiquark annihilation from the simulation[27, 28]. The strange mass $am_s = 0.030$ gives the fictitious pseudoscalar $s\bar{s}$ mass $m_{s\bar{s}} = 682$ MeV (with $a = 0.13$ fm) which corresponds to the bare strange mass $m_s = 45.46$ MeV on $20^3 \times 64$ lattice. With that fitted strange mass, the vector meson $\phi = s\bar{s}$ is found to have $m_\phi \approx 1120$ MeV[PDG[33] value 1020 MeV]. According to leading order chiral perturbation theory, vector kaon mass (m_{K^*}) and the square of the pseudoscalar kaon mass ($m_K^2 = m_{K^\pm}^2 = m_{K^0}^2$) depend linearly on the quark mass: $m_{K^*} = \lambda + \lambda_2(m + m_s)$ and $m_K^2 = B(m + m_s)$. In Fig.7, m_K^2 and m_{K^*} for the above mentioned strange mass are plotted against the lighter quark masses. The lightest pion mass

in the plot is $m_\pi \approx 400$ MeV (corresponding to the light quark mass $am = 0.01$). For this pion mass, ρ mass is found to be $m_\rho = 912$ MeV and the kaon masses on this coarse lattice are obtained as $m_K \approx 550$ MeV[PDG value 496 MeV] and $m_{K^*} \approx 1035$ MeV[PDG value 892 MeV].

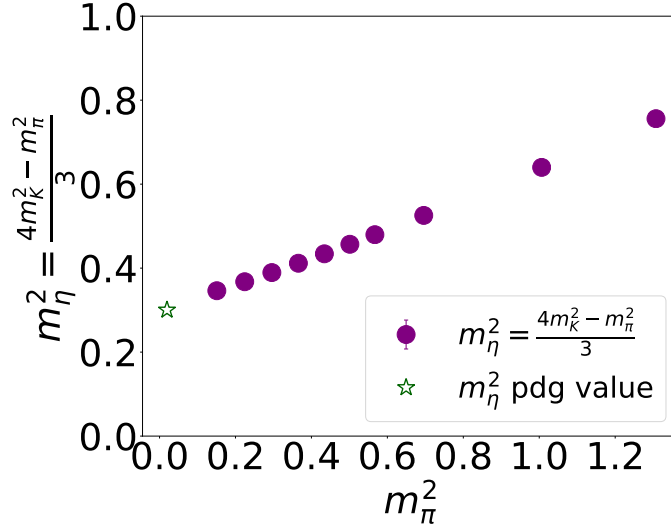


FIG. 8: The η mass from GMOR relation on $20^3 \times 64$ lattice. The star symbol (\star) in the figure indicates the PDG value of m_η at $m_\pi = 140$ MeV.

A consequence of the approximate chiral symmetry in QCD is the Gell-Mann-Oakes-Renner(GMOR) relation. In the leading order of chiral perturbation theory, the GMOR relation translates into the Gell-Mann Okubo mass formula for pseudoscalar mesons which can be written as

$$3m_\eta^2 = 4m_K^2 - m_\pi^2. \quad (10)$$

In Fig.8, we have shown the GMOR relation for different pion masses. Another interesting mass formula which is also found to be reasonably satisfied by the meson spectrum was obtained in the $SU(6)$ theory. The $SU(6)$ mass formula [34] relates the vector-pseudoscalar splittings as:

$$m_{K^*}^2 - m_K^2 = m_\rho^2 - m_\pi^2. \quad (11)$$

The above $SU(6)$ relation was shown to deviate on lattice with increasing quark mass[35]. In Fig.9, we have shown the variations of the vector-pseudoscalar splittings with the pion

mass. We have also plotted the ratio $(m_V^2 - m_{PS}^2)/M_K^2$ for strange and non-strange sectors against m_{PS}^2/M_K^2 where M_K is the PDG value of the kaon mass, m_V is m_{K^*} and m_ρ when m_{PS} is m_K and m_π respectively.

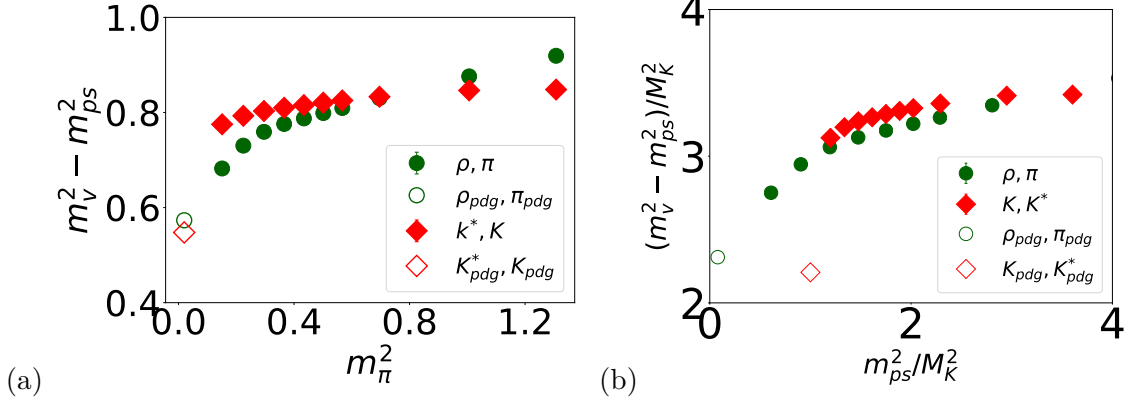


FIG. 9: (a) The vector-pseudovector mass splitting $m_V^2 - m_{PS}^2$ is plotted with m_π^2 . The $SU(6)$ mass formula is approached with decreasing pion mass (PDG values of the splittings are indicated by open circle and open diamond). (b) The ratio $(m_V^2 - m_{PS}^2)/M_K^2$ is plotted with m_{PS}^2/M_K^2 where M_K is the PDG value of the kaon mass. The result is from $20^3 \times 64$ lattice.

V. PARTIAL QUENCHING AND THE SCALAR CORRELATOR

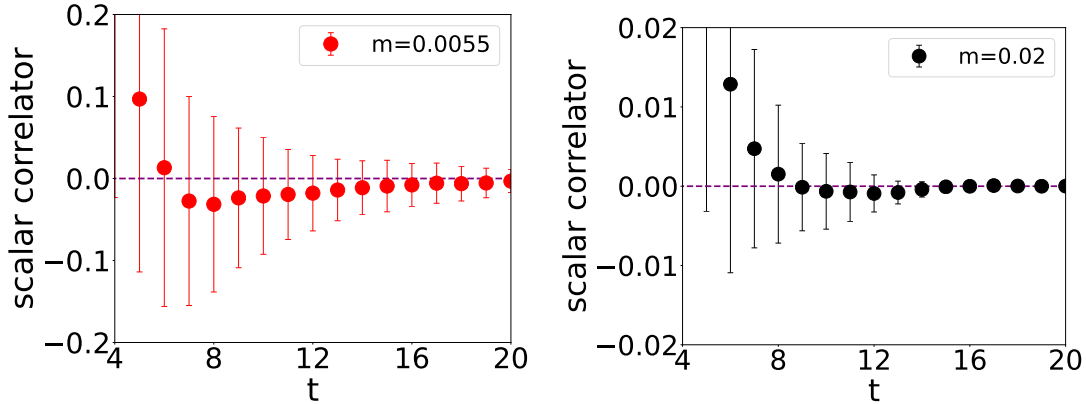


FIG. 10: Scalar correlator for two different valence masses $m_{\text{val}} = 0.0055$ and $m_{\text{val}} = 0.02$ with sea mass $m_{\text{sea}} = 0.01$, for nonperturbatively tuned value of the counter term $\tilde{c}_3 = -0.05$.

Lattice QCD with mixed action is inevitably partially quenched, no choice of valence quark mass can completely remove unitarity violating effects from mixed action theory at nonzero lattice spacing. The full QCD can be recovered in the continuum limit only.

The scalar meson ($\bar{\psi}\psi$) is known to be sensitive to this unitary violation, it gives the scalar correlator a negative value when valence quark mass is less than sea quark. The two point correlator should be positive for dynamical fermions in full QCD where unitarity is preserved. But in the partial quenched QCD when $m_{\text{val}} < m_{\text{sea}}$, the flavor neutral two-meson intermediate state couples to the scalar meson correlator with a negative weight. However, when $m_{\text{val}} > m_{\text{sea}}$, the one loop contribution to the scalar correlator coming from the exchange of the two-meson fields becomes positive [36].

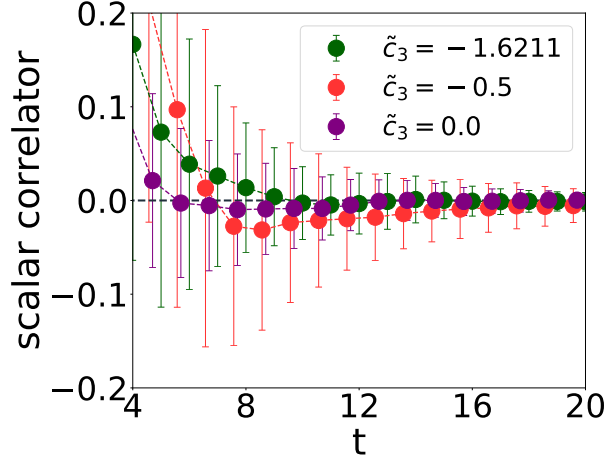


FIG. 11: Scalar correlator for different values of \tilde{c}_3 for $m_{\text{val}} < m_{\text{sea}}$. The lines connecting the points are to guide the eyes.

This effect of partial quenching is shown in Fig. 10, which is observed when the parity breaking is minimized by non-perturbative tuning of \tilde{c}_3 . The errors become large for partially quenched scalar correlators, but its negative value when $m_{\text{val}} (= 0.005) < m_{\text{sea}} (= 0.01)$ is observable. From the plot for $\tilde{c}_3 = -0.5$, it is evident that as one increases valence quark mass, for a fixed sea quark mass, the negative contribution reduces. By looking at the sign of the scalar correlator as the mass of valence quark is changed, it should be possible to match the valence and sea quark masses. In the plots for \tilde{c}_3 away from non-perturbative value, *i.e.* in presence of parity breaking we do not see this effect of negative contribution. In Fig.11, the scalar correlators for different values of \tilde{c}_3 are compared to demonstrate that the partial quenching sets in when the counter term restores the parity. On the question whether we can also have negative scalar correlators in the parity broken phase, we cannot be definitive at this stage since relevant mixed action ChiPT involving BC fermions on staggered sea has not been worked out as yet. All we can emphasize at the moment is that our numerical

data shows, in spite of large errorbars, in broken symmetric phase the mean of the scalar correlators are never negative over a range of $m_{val} \lesssim m_{sea}$. Nevertheless, to understand the sign of scalar correlators in various phases, we certainly need corresponding mixed action ChiPT.

VI. Δ_{mix}

In mixed action calculations, we can have three different types of mesons: mesons composed of (i) two valence quarks, (ii) two sea quarks and (iii) a mix of one valence and one sea quark. Each of these undergo lattice spacing dependent mass renormalization. The mixed action χ PT in leading order has an $\mathcal{O}(a^2)$ dependent low energy constant Δ_{mix} . The degree of unitarity violation at finite lattice spacing depends on the size of Δ_{mix} . In the leading order, the pseudoscalar meson masses for BC valence and Asqtad sea are given by

$$m_{v_1 v_2}^2 = B_v(m_{v_1} + m_{v_2}) \quad (12)$$

$$m_{s_1 s_2, t}^2 = B_0(m_{s_1} + m_{s_2}) + a^2 \Delta_t \quad (13)$$

$$m_{vs}^2 = B_v m_v + B_0 m_s + a^2 \tilde{\Delta}_{\text{mix}}, \quad (14)$$

where $m_{v_1 v_2}$ ($m_{s_1 s_2}$) is the pseudoscalar meson mass made up of valence (sea) quark and antiquark while m_{vs} is the mass of the mixed meson composed of valence and sea quarks. The $a^2 \Delta_t$ are the taste splittings of the *staggered* pions, where $t = A, T, V, I$ and $a^2 \Delta_5 = 0$ [37] and $a^2 \tilde{\Delta}_{\text{mix}} = a^2 \Delta_{\text{mix}} + a^2 \Delta'_{\text{mix}}$ where [38],

$$a^2 \Delta'_{\text{mix}} = \frac{1}{8} a^2 \Delta_A + \frac{3}{16} a^2 \Delta_T + \frac{1}{8} a^2 \Delta_V + \frac{1}{32} a^2 \Delta_I. \quad (15)$$

The different renormalizations of the quark masses in different actions are absorbed in the coefficients B_0 and B_v . The $\tilde{\Delta}_{\text{mix}}$ can be extracted from the meson spectrum data from either of the following ways,

$$m_{vs}^2 - \frac{1}{2} m_{vv}^2 = B_0 m_s + a^2 \tilde{\Delta}_{\text{mix}} \quad \text{or} \quad (16)$$

$$\delta m^2 \equiv m_{vs}^2 - \frac{1}{2} m_{ss,5}^2 = B_v m_v + a^2 \tilde{\Delta}_{\text{mix}}. \quad (17)$$

It is convenient to work with the form in Eq. 17 as there are more m_v available (than m_s) for a good linear fit. The Fig. 12 shows the result of variation of δm^2 with m_v and the linear extrapolation of δm^2 in the bare valence mass m_v gives the $a^2 \tilde{\Delta}_{\text{mix}}$ as the y -intercept. To

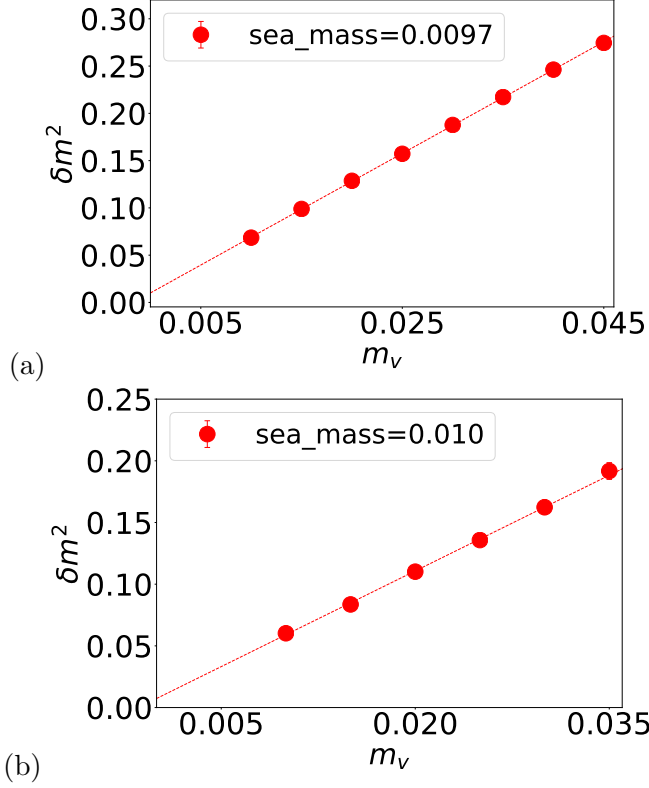


FIG. 12: $\delta m^2 = m_{vs}^2 - \frac{1}{2}m_{ss}^2$ plotted as a function of m_v (a) $16^3 \times 48$ lattice with $m_s = 0.0097$, (b) $20^3 \times 64$ lattice with $m_s = 0.01$. The intercept on the δm^2 axis gives the value of $\tilde{\Delta}_{mix}$.

determine the actual size of unitarity violation due to differences in valence and sea quark discretization, one needs to subtract the taste splitting dependent terms in Eq. 15 [13, 39].

The values of $\tilde{\Delta}_{mix}$ have been tabulated and compared with other works in Table III. For the form of $a^2\Delta'_{mix}$ for Wilson sea fermions see [39]. The value of $\tilde{\Delta}_{mix}$ obtained in this work is rather encouraging. Although our value appears smaller than the studies with domain wall fermion on staggered sea [13, 14], a direct comparison with it is difficult because of our coarser lattices, less statistics, fitting strategy and no systematic error estimation. Note that we feature the results for $\tilde{\Delta}_{mix}$ that includes the Δ'_{mix} , which in our case contains contribution from the taste splitting. Still, the lattice artifact $\tilde{\Delta}_{mix}$, measuring the size of unitarity violation in our mixed action lattice simulations with Borici-Creutz fermions on staggered sea, is of the same order of magnitude as the rest.

Mixed action	a fm	$\tilde{\Delta}_{mix}$ GeV ⁴
Overlap on Clover[15]	0.09	0.55(23)
DWF on staggered[14]	0.125	0.249(6)
DWF on staggered[13]	0.12	0.211(16)
DWF on staggered[13]	0.09	0.173(39)
Overlap on DWF[17]	0.114	0.030(6)
Overlap on DWF[17]	0.085	0.033(12)
Overlap on HISQ [40]	0.12	0.112(11)
BC on staggered[this work]	0.15	0.03(1)
BC on staggered[this work]	0.13	0.03(8)

TABLE III: $\tilde{\Delta}_{mix}$ for different mixed actions with 300 MeV pion mass.

VII. SUMMARY AND CONCLUSIONS

Mixed action lattice QCD is commonly employed to compute hadronic observables as it allows use of numerically cheaper lattice fermions in the sea sector while using chirally improved, and possibly expensive, valence fermions. Such mixed action approach is also rather expedient when a new fermion discretization, Borici-Creutz fermions in the present case, is tried for lattice calculations. In this paper, we presented the first results for light hadron mass spectrum and mixed action parameter Δ_{mix} using Borici-Creutz valence fermion on staggered sea.

As a first step, we nonperturbatively tuned the two counterterm coefficients \tilde{c}_3 and c_4 to restore the parity and time symmetry, which are otherwise broken by Borici-Creutz action. We found that the tuned values of $\tilde{c}_3 = -0.50$, $c_4 = 0.005$ are significantly different from the perturbative estimates (given in Table II). We observed that the tuning of \tilde{c}_3 and c_4 can proceed independently of each other. The \tilde{c}_3 is tuned by minimizing the value of parity condensate $|\langle i \bar{\psi} \gamma_5 \tau^3 \psi \rangle|$. The variation of parity condensate with \tilde{c}_3 is found to be insensitive to variation of c_4 over the range $[0.005, 0.1]$ and three different lattice spacings 0.15 fm, 0.13 fm, 0.09 fm.

In a (discretized) Lorentz invariant theory, the forward and backward propagating pions are the same and have the same masses. But with the Borici-Creutz action this has to

be achieved by tuning the counterterm coefficients by minimizing the mass differences of the forward and backward propagating pions. We observed that the forward-backward symmetry, *i.e.* the time symmetry, is attained entirely by tuning c_4 , independent of \tilde{c}_3 over the range $[-1.8, -0.4]$. The term containing c_4 is a kinetic ‘like’ term and, therefore, expected to influence the correlation of operators separated over time. This might be the reason we see pion correlation function propagating differently in opposite time direction. We must clarify that this differently propagating pion in time is not the same as opposite parity baryon and antibaryon propagating forward and backward in time.

The tuned values of \tilde{c}_3 and c_4 seem to have very small dependence on the lattice spacings. This is perhaps expected since the observables used for tuning are not known to have significant cut-off effect. We don’t expect these tuned values to change much with different m_l/m_s and physical volumes but certainly will depend on the variant of sea fermions.

Once the counterterms are nonperturbatively tuned, we studied the variation of pion mass m_π with the bare valence quark masses m in the range $[0.007 - 0.5]$. The plot m_π^2 versus m in Fig. 6 shows almost linear behavior in the entire range of quark mass except near small masses. The partially quenched chiral log is most visible in the plot m_π^2/m versus m , the behavior of which can be described by PQ χ PT formula Eq. 9. Since we did not use simultaneous *i.e.* global fit over all the ensembles, we cannot comment much on the parameters C_i ’s of Eq. 9. They are used only for fitting purpose and hence not quoted. The chiral log plot has been used in [17] to determine the range of quark masses where LO MA χ PT relation(s) can be used. In our case, we used both m_π^2 vs m and m_π^2/m vs m plots to determine the valence quark mass range. It is to be noted that the mass tuning in mixed action simulation is not unique and for any choice the mixed action will violate unitarity at finite lattice spacing and all partial quenching pathologies will show up. For instance, this tuning can also be done by matching the pion mass in valence sector to the pion mass in the sea sector. Hence, in this work we chose quark masses that are just outside the region of chiral log, ensure that $m_\pi L \geq 4$ and $m_{\text{val}} \gtrsim m_{\text{sea}}$.

The scalar correlators, plotted in Figs. 10 shows the unitarity violating effects in the mixed action theory. However, unlike other mixed action scalar correlator plots, there is an extra complication in the behavior of the scalar correlators – it is the role of the counterterm \tilde{c}_3 . The term $\tilde{c}_3 \bar{\psi} \Gamma \psi$, is like a mass ‘like’ term and, as a result, we do not see an ‘absolute’ clear negative values in the scalar correlators. In the plot for $\tilde{c}_3 = -0.5$, the

scalar correlator for $m = 0.0055$ ($< m_l$) has negative mean values but the error bars are large implying correlators varying over a range of positive and negative values. But, when $m = 0.02$ ($> m_l$), the correlator points are distinctly in the positive region. From the other plot with $m = 0.0055$ and $\tilde{c}_3 = -1.6211$, where parity is only partially restored, we find that \tilde{c}_3 is driving the scalar correlators towards positive value regardless the fact $m < m_l$. An MA χ PT for Borici-Creutz valence fermion on staggered sea, which is presently not available, can only tell us exactly how this is achieved.

Finally, we want to determine the size of unitarity violation by measuring the mixed valence-sea meson mass splitting Δ_{mix} . This is an important lattice artifact to determine for any mixed action calculations. In this paper we actually measured the $\tilde{\Delta}_{\text{mix}}$, which contains an additional lattice spacing dependent term Δ'_{mix} containing the contributions of the taste splittings. For pion mass about 300 MeV, we obtained $\tilde{\Delta}_{\text{mix}} = 0.03(1) \text{ (GeV)}^4$ at $a = 0.15$ fm and $0.03(8) \text{ (GeV)}^4$ at $a = 0.13$ fm, *i.e.* they are same within the error. This result is at par (same order of magnitude) with the other mixed action studies as tabulated in Table III. However, the fits that are performed here to arrive at these results are all uncorrelated and no global fitting (involving all the ensemble data) are performed. Thus the mean value and error bar of $\tilde{\Delta}_{\text{mix}}$ can change depending on more sophisticated fitting procedure. But we expect it not to be substantial. Based on this observation, we can certainly claim that this is an encouraging first result for Borici-Creutz fermion when compared to other mixed action studies. It is worth following up the study of Borici-Creutz fermion more rigorously and attempt a fully unquenched lattice QCD investigation.

Acknowledgements: The numerical jobs have been run on the HPC at IIT Kanpur funded by DST and IIT Kanpur and on computer facility at NISER, Bhubaneswar. One of the authors (SB) thanks DST-SERB for providing fund (project number SR/S2/HEP-0025/2010) for computers in which a part of this work is carried out and JG thanks Rudina Zeqirllari for useful communications.

-
- [1] L.H. Karsten, Phys. Lett. B **104**,315 (1981).
 - [2] F. Wilczek, Phys. Rev. Lett. **59**,2397 (1987).
 - [3] M. Creutz, JHEP **0804**, 017(2008).

- [4] A. Borici, Phys. Rev. D. **78**, 074504 (2008).
- [5] P.F. Bedaque, M.I. Buchoff, B.C. Tiburzi, A. Walker-Loud, Phys. Lett. B. **662**, 449 (2008).
- [6] M. Creutz, Pos LATTICE **2008**, 080 (2008).
- [7] S. Capitani, J. Weber and H. Wittig, Phys. Lett. B **681**, 105 (2009).
- [8] S. Capitani, M. Creutz, J. Weber, H. Wittig, JHEP **1009**, 027 (2010).
- [9] D. Chakrabarti, S.J. Hands, A. Rago, JHEP **0906**, 060 (2009).
- [10] K. Cichy, J. Gonzalez Lopez, K. Jansen, A. Kujawa and A. Shindler, Nucl. Phys. B **800**, 94 (2008).
- [11] J. Goswami, D. Chakrabarti, S. Basak, Phys. Rev. D **91**, no. 1, 014507 (2015)
- [12] J. Goswami, D. Chakrabarti, S. Basak, Int. J. Mod. Phys. A **32**, 1750059 (2017).
- [13] C. Aubin, J. Laiho and R.S. Van de Water, Phys. Rev. D **77**, 114501 (2008).
- [14] K. Orginos, A. Walker-Loud, Phys. Rev. D **77**, 094505 (2008).
- [15] S. Durr *et al.*, PoS LATTICE **2007**, 115 (2007).
- [16] A. Li *et al.* [xQCD Collaboration], Phys. Rev. D **82**, 114501 (2010).
- [17] M. Lujan *et al.*, Phys. Rev. D **86**, 014501 (2012).
- [18] O. Bär, M. Golterman, Y. Shmir, Phys. Rev. D **83**, 054501 (2011).
- [19] S.R. Beane, P.F. Bedaque, K. Orginos, M.J. Savage, Phys. Rev. D **73**, 054503 (2006); Phys. Rev. Lett. **97**, 012001 (2006).
- [20] R. G. Edwards *et al.* (LHPC Collaboration), Phys. Rev. Lett. **96**, 052001 (2006).
- [21] S. Prelovsek, Phys. Rev. D **73**, 014506 (2006).
- [22] K. Cichy, V. Drach, E. Garcia-Ramos, G. Herdoiza and K. Jansen, Nucl. Phys. B **869**, 131 (2013).
- [23] K. Ottnad, C. Urbach, F. Zimmermann, Nucl. Phys. B **896**, 470 (2015).
- [24] M. Creutz, PoS LATTICE **2010**, 078 (2010).
- [25] B. C. Tiburzi, Phys. Rev. D **82**, 034511 (2010).
- [26] R. Zeqirllari, Private communication; A. Borici, R. Zeqirllari, *Buletini i Shkencave Natyrore, Universiteti i Tiranës, Nr 19*, pp. 145–150, 2015.
- [27] C.W. Bernard *et al.*, Phys. Rev. D **64**, 054506 (2001).
- [28] C.T.H. Davies *et al.* [HPQCD Collaboration], Phys. Rev. D **81**, 034506 (2010).
- [29] C. Aubin *et al.*, Nucl. Phys. (Proc. Suppl.) **119**, 233 (2003).
- [30] Y. Chen, S.J. Dong, T. Draper, I. Horvath, F.X. Lee, K.F. Liu, N. Mathur, J.B. Zhang, Phys.

- Rev. D **70**, 034502 (2004).
- [31] S. Basak, S. Datta, M. Padmanath, P. Majumdar, N. Mathur, PoS LATTICE **2012**, 141 (2012).
 - [32] S.R. Sharpe, Phys. Rev. D **56**, 7052 (1997) Erratum: [Phys. Rev. D **62**, 099901 (2000)].
 - [33] C. Patrignani *et al.* [Particle Data Group], Chin. Phys. C **40**, no. 10, 100001 (2016).
 - [34] A. Pais, Phys. Rev. Lett. **13**, 175 (1964).
 - [35] S. Aoki *et al.* [CP-PACS Collaboration], Nucl. Phys. Proc. Suppl. **63**, 161 (1998).
 - [36] S. Prelovsek, C. Dawson, T. Izubuchi, K. Orginos, A. Soni, Phys. Rev. D **70**, 094503 (2004).
 - [37] C. Aubin *et al.* [MILC Collaboration], Phys. Rev. D **70**, 114501 (2004).
 - [38] M. Golterman, [arXiv:0912.4042](https://arxiv.org/abs/0912.4042) [hep-lat].
 - [39] J.W. Chen, M. Golterman, D. O'Connell, A. Walker-Loud, Phys. Rev. D **79**, 117502 (2009).
 - [40] S. Basak *et al.* [ILGTI Collaboration], PoS LATTICE **2014**, 083 (2015).